ARTICLE
Journal of Cellular Biochemistry 109:915–926 (2010)

Journal of Cellular Biochemistry

# SUV39h- and A-Type Lamin-Dependent Telomere Nuclear Rearrangement

Radka Uhlířová,[1] Andrea Harničarová Horáková,[1] Gabriela Galiová,[1] Soňa Legartová,[1] Pavel Matula,[1,2] Miloslava Fojtová,[1,3] Miroslav Vařecha,[2] Jana Amrichová,[2] Jan Vondráček,[1] Stanislav Kozubek,[1] and Eva Bártová[1*]

[1]*Institute of Biophysics, Academy of Sciences of the Czech Republic, v.v.i., Královopolská 135, CZ-612 65 Brno, Czech Republic*

[2]*Faculty of Informatics, Masaryk University, Botanická 68a, CZ-602 00 Brno, Czech Republic*

[3]*Department of Functional Genomics and Proteomics, Institute of Experimental Biology, Faculty of Sciences, Masaryk University Brno, Kotlářská 2, CZ-611 37 Brno, Czech Republic*

## ABSTRACT

Telomeres are specialized chromatin structures that are situated at the end of linear chromosomes and play an important role in cell senescence and immortalization. Here, we investigated whether changes in histone signature influence the nuclear arrangement and positioning of telomeres. Analysis of mouse embryonic fibroblasts revealed that telomeres were organized into specific clusters that partially associated with centromeric clusters. This nuclear arrangement was influenced by deficiency of the histone methyltransferase SUV39h, LMNA deficiency, and the histone deacetylase inhibitor Trichostatin A (TSA). Similarly, nuclear radial distributions of telomeric clusters were preferentially influenced by TSA, which caused relocation of telomeres closer to the nuclear center. Telomeres also co-localized with promyelocytic leukemia bodies (PML). This association was increased by SUV39h deficiency and decreased by LMNA deficiency. These differences could be explained by differing levels of the telomerase subunit, TERT, in SUV39h- and LMNA-deficient fibroblasts. Taken together, our data show that SUV39h and A-type lamins likely play a key role in telomere maintenance and telomere nuclear architecture. J. Cell. Biochem. 109: 915–926, 2010. 

**KEY WORDS:** SUV39H; HISTONE METHYLTRANSFERASES; TELOMERES; PML BODIES; LMNA GENE; EPIGENETICS; CHROMATIN STRUCTURE; NUCLEAR RADIAL DISTRIBUTIONS; IMAGE ANALYSIS

Telomeres are present at the ends of metaphase chromosomes and consist of DNA and specific telomere-binding proteins. Telomeric DNA is composed of repetitive TTAGGG sequences that attract a specific protein complex known as shelterin (telosome), preventing the chromosome ends from undergoing undesirable recombination, repair, or end-to-end fusion. Telomeres are highly specialized chromatin structures that are shortened with each cell division. Thus, telomere length restricts the number of replications, with this restriction being associated with a cell growth limit known as replicative senescence. Telomere repeats are generated by telomerase reverse transcriptase (TERT), which recognizes chromosome ends and synthesizes telomere repeats de novo using a telomerase-associated RNA molecule (TERC) as a template [summarized by Blasco, 2007a,b]. The TERT-TERC telomerase complex is stabilized by dyskerin (Dkc1) (Fig. 1A). Contrary to standard telomere maintenance in somatic cells, telomere synthesis in some immortalized human cell lines and tumor cells occurs in the absence of telomerase activity through a mechanism called alternative lengthening of telomeres (ALT) [summarized by Lundblad, 2002; Muntoni and Reddel, 2005]. This mechanism involves recombination between telomeric sequences [Henson et al., 2002] and generates heterogenous telomere lengths, a feature especially evident in tumor cells. The main hallmark of ALT is the presence of ALT-associated promyelocytic leukemia (PML) bodies, which

Abbreviations used: 3D, three-dimensional; dn, double null; H3, histone H3; HMTs, histone methyltransferases; HP1, heterochromatin protein 1; MEFs, mouse embryonic fibroblasts; PML bodies, promyelocytic leukemia bodies; RT, room temperature; wt, wild type; TSA, Trichostatin A; TERT, telomerase reverse transcriptase; TERC, telomerase-associated RNA molecule; Dkc1, dyskerin; ALT, alternative lengthening of telomeres; TRF1 and TRF2, telomere repeat binding factors 1 and 2; Pot1, protection of telomeres 1 protein.

*Correspondence to: Dr. Eva Bártová, Institute of Biophysics, Academy of Sciences of the Czech Republic, v.v.i., Královopolská 135, CZ-612 65 Brno, Czech Republic. E-mail: bartova@ibp.cz

Received 11 October 2009; Accepted 23 November 2009 • DOI 10.1002/jcb.22466 • © 2010 Wiley-Liss, Inc.
Published online 12 January 2010 in Wiley InterScience (www.interscience.wiley.com).

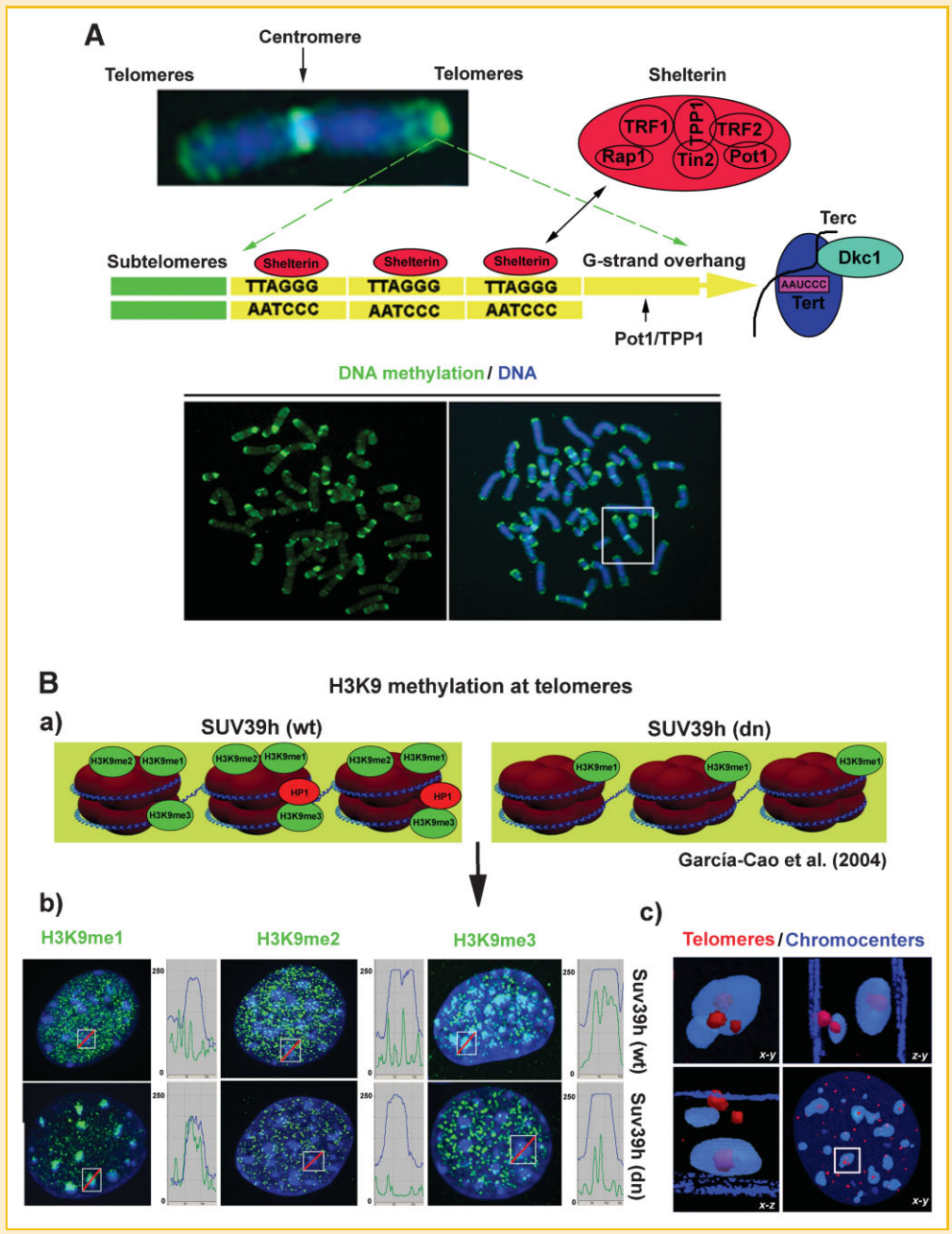


Fig. 1. Structure and epigenetics of telomeres. A: Telomeres are highly methylated nucleoprotein complexes that maintain the integrity of genetic information. Human telomeres consist of TTAGGG repeats that are protected by several proteins (TRF1, TRF2, Pot1, Tin2, Rap1, and TPP1) that make up the shelterin–telosome complex. Elongation of telomeres is mediated by telomerase, which contains of the two essential subunits, TERT and TERC. Telomerase also contains one molecule of dyskerin (Dkc1), a protein that stabilizes the telomerase complex. Ba: Telomeres are characterized by a specific epigenetic pattern. These structures are densely H3K9 mono-, di-, and tri-methylated. Deficiency of the HMTs, SUV39h, causes the loss of H3K9 di- and tri-methylation as well as HP1 protein in this genomic region [García-Cao et al., 2004]. Bb: Epigenetic changes at chromocenters induced by SUV39h deficiency likely influence the epigenetic pattern of telomeres. The fluorescence intensity of selected chromocenters was quantified using Andor iQ software. Fluorescence intensities (in RGB mode) were estimated along the red line in the white frame for individual chromocenters. In chromocenters of SUV39h-deficient cells, H3K9me1 was increased, while H3K9me2 and H3K9me3 were decreased. Bc: Animation by ImageSurfer (http://152.19.37.82/main) showing the formation of telomere clusters (red), which associate with clusters of centromeres called chromocenters (blue foci).

co-localize with telomeric DNA, telomere-binding proteins, and proteins involved in DNA synthesis and recombination [Yeager et al., 1999]. This interaction is highly dynamic despite the relative immobility of PML bodies [Molenaar et al., 2003]. Therefore, understanding the interaction between telomeres and ALT-associated PML bodies may be useful for tailoring anti-cancer therapies directed towards cells undergoing ALT.

Mammalian telomeres terminate in G-rich 3′ overhangs that are generated by post-replicative events at the C-rich strand [Bailey et al., 2001]. G-strand overhangs (Fig. 1A) provide a template for

telomerase-mediated telomere elongation and can form so-called t-loops and/or t-circles [Muntoni and Reddel, 2005] that protect telomeres from being recognized as DNA breaks [de Lange, 2004]. The shelterin complex that is attracted to the terminal ends of telomeres, consists of protection of telomeres 1 protein (Pot1), TPP1 heterodimer, telomere repeat binding factors (TRF1 and TRF2), a TRF-interacting partner known as repressor activator protein 1 (Rap1), and TRF1-interacting nuclear protein 2 (Tin2) (Fig. 1A). TRF1 likely regulates telomere length and prevents fusion of telomere ends [van Steensel et al., 1998; Celli and de Lange, 2005] associated with homologous recombination and DNA repair processes such as non-homologous end joining. Like Pot1, TRF2 prevents the DNA damage response from occurring at telomeres [Karlseder et al., 2004]. The shelterin complex is also closely related to densely tri-methylated histone H3 at lysine 9 (H3K9me3) and H4K20me3 at telomeres [García-Cao et al., 2004; Blasco, 2007a]. Moreover, sub-types of heterochromatin protein 1 (HP1α, HP1β, HP1γ) bind to H3K9-methylated regions in telomeres. [Gonzalo et al., 2005, 2006; Fig. 1A,B]. Interestingly, cells deficient in SUV39h1 and SUV39h2, the histone methyltransferases (HMTs) responsible for H3K9 methylation, have abnormally long telomeres. Moreover, these cells are characterized by a reduced level of H3K9me2 and H3K9me3, while H3K9me1 levels remain unchanged at telomeric regions [García-Cao et al., 2004; Fig. 1Ba]. This phenomenon could be related to a SUV39h-dependent decrease in H3K9me2 and H3K9me3 as well as a SUV39h-dependent increase in H3K9me1 occurring at pericentromeric clusters (i.e., chromocenters) [Schotta et al., 2004], which significantly associate with telomeres (see Fig. 1Bb,Bc). These data clearly show that a close relationship exists between telomere maintenance and histone signatures. This close relationship is supported by findings concerning age-related pathologies. For example, a number of age-related pathologies, such as distinct laminopathies and premature aging, are characterized by telomere shortening. Moreover, laminopathies such as premature aging and diseases caused by mutations in the A-type lamin gene are accompanied by changes in the histone signature, such as altered levels of H3K9me3 and H4K20me3, as well as decreased levels of HP1 protein sub-types (HP1γ). These changes have been observed in Hutchinson-Gilford Progeria Syndrome (HGPS) [Scaffidi and Misteli, 2006; Shumaker et al., 2006]. Thus, a close relationship exists among the histone signature, telomere maintenance, and A-type lamin function.

An important feature of telomeres is their ability to silence genes in close proximity to telomere repeats [Gottschling et al., 1990; Cryderman et al., 1999]. This phenomenon is called the telomere position effect (TPE) [Baur et al., 2001; Ning et al., 2003]. Interactions between genes and telomeres [Molenaar et al., 2003] likely play an important role in nuclear organization [Nagele et al., 2001]. However, findings related to telomere nuclear positioning have been ambiguous. In human cells, telomeres were described to be randomly positioned throughout the interphase nucleus by Ludérus et al. [1996]. Conversely, Amrichová et al. [2003] reported that telomeres adopt a polar orientation within chromosome territories, with these structures being opposite to centromeric sequences. Remarkably, some data have shown that telomeres are important for the nuclear positioning of chromosome territories owing to telomere attachment to hypothetical nuclear matrix [Weipoltshammer et al., 1999]. Given these findings, we investigated how changes in histone signature and A-type lamin deficiency influence telomere nuclear radial arrangement, clustering, length, and association with the PML body compartment.

## MATERIALS AND METHODS

### CELL CULTURES AND FLOW CYTOMETRY

We used mouse embryonic fibroblasts (MEFs) from wild type (wt) and SUV39h double null (dn) mice. SUV39h mice originated from the laboratory of Prof. Thomas Jenuwein at Max-Planck Institute of Immunobiology, Freiburg, Germany. The cells were cultivated in high glucose DMEM (#D1152, Sigma–Aldrich, CZ) supplemented with 10% fetal calf serum (PAN, Germany), 100 i.u./ml penicillin, and 0.1 mg/ml streptomycin. Medium contained 1 μl β-mercaptoethanol (Gibco, #31350-010), 5 ml non-essential amino acids (100×) (Gibco, #11140-035), 5 ml sodium pyruvate (Gibco, #11360-039), and 1.5 g $NaHCO_3$. At 70% confluence, the cells were treated with a final concentration of 100 nM Trichostatin A (TSA). Cells were cultured under standard conditions at 37°C in a humidified atmosphere containing 5% $CO_2$. Immortalized (dn) MEFs for the A-type lamin gene, *LMNA*, as well as (wt) MEFs were a generous gift from Dr. Teresa Sullivan and Prof. Collin L. Stewart from the Institute of Medical Biology in Singapore. These cells were cultured in high glucose D-MEM supplemented with 10% of fetal bovine serum under standard conditions.

For flow cytometry, the cells were fixed in 70% ethanol and stored at −20°C. Prior to use, the cells were washed twice in PBS and stained with propidium iodide (10 μg/ml), dissolved in Vindelov solution [1 mM Tris–HCl (pH 8.0), 1 mM NaCl, 0.1% TritonX-100, 10 μg/ml RNase A]. Cells were then incubated for 30 min at 37°C. Cell cycle profiles were measured using the FASCalibur flow cytometer (Becton Dickinson, Franklin Lakes, NJ), controlled by CellQuest software running on an Apple Macintosh computer. The number of cells in each cell cycle phase was determined using ModFit software (Verity Software House, Topsham, ME).

### IMMUNOFLUORESCENCE

Cells were fixed with 4% paraformaldehyde for 10 min at room temperature (RT). Immunofluorescence was performed according to Bártová et al. [2005] using rabbit polyclonal antibody to Rap1 (#ab4181, Abcam) and mouse monoclonal antibody to PML (#K0196-3, MBL, Medical & Biological Laboratories, Co., LTD, Japan). After incubation with primary antibody, the cells were washed twice in PBS for 5 min and incubated for 1 h at RT with goat anti-mouse Alexa Fluor 594 (Molecular Probes, Invitrogen) and/or with goat anti-rabbit Alexa Fluor 488 (Molecular Probes, Invitrogen). Secondary antibodies were diluted 1:200 in 1% BSA dissolved in PBS. Immunostained cells were then washed three times in PBS for 5 min and counterstained with TO-PRO-3 iodide (0.04 μg/ml, Molecular Probes).

## FISH TECHNIQUE

Cells were fixed on microscopic slides with 4% paraformaldehyde for 8 min at RT and washed in PBS three times for 2 min. The DNA-FISH procedure was then performed as described elsewhere [Harničarová et al., 2006]. DNA probe for all telomeric regions was prepared according to the method of Ijdo et al. [1991]. Briefly, PCR was carried out in the absence of template using the primers $(TTAGGG)_5$ and $(CCCTAA)_5$. PCR was performed in PCR buffer (50 mM KCl; 10 mM Tris–HCl, pH 8.3; 1.5 mM $MgCl_2$), 200 μM of each dNTP, 0.1 μM of each primer, and 2 U of Combi Taq DNA polymerase (Top-Bio, Czech Republic) in a total volume 50 μl. Amplification was performed using 10 cycles at 94°C/1 min, 55°C/30 s, and 72°C/1 min; 30 cycles at 94°C/1 min, 60°C/30 s, and 72°C/90 s; and then a final extension at 70°C for 5 min. PCR products were analyzed by agarose gel electrophoresis. PCR products were purified using the QIAguick PCR purification kit (#28104, Qiagen, Bio-Consult, Czech Republic), and standard Nick translation was performed as described by Harničarová et al. [2006]. FISH signals were visualized using rhodamine-conjugated anti-digoxigenin (Roche, Czech Republic). The preparations were then washed in 4× SSC/0.2% Igepal (three times for 4 min at 37°C and once for 4 min at RT) and counterstained with TO-PRO-3 (0.4 μg/ml).

## IMAGE ACQUISITION AND SOFTWARE

High-resolution image acquisition was performed using a Nipkow disc-based confocal microscope system as described elsewhere [Amrichová et al., 2003; Bártová et al., 2005; Harničarová et al., 2006]. The image acquisition system was controlled by Acquiarium software. Both image analysis and three-dimensional (3D) image visualization was performed using this software [see Matula et al., 2009 and http://cbia.fi.muni.cz/acquiarium/].

For analysis of the 3D nuclear radial distribution of individual telomeres and their clusters, cell nuclei were segmented using a threshold-based method. The threshold was automatically computed according to the Otsu method [Otsu, 1979]. The position of the telomeres was computed using a mathematical morphology approach based on the EMAX transformation [Soille, 2004]. We studied the relative position of telomeres inside the nuclei of mouse fibroblasts by means of the local radius, which was defined in a way to make it suitable for flat objects. We denoted the local radius for flat objects as the *FLR* measure. The *FLR* measure was equal to 0% for points in the geometric center of the nucleus and 100% for points next to the nucleus membrane. An example of the *FLR* measures for a typical nucleus that is divided into 10 zones (each spanning a distance of 10%) is depicted in Figure 2. The *FLR* measure was computed using Acquiarium software.

The FLR measure is defined as follows. Q is the point inside the nucleus that is equal to $(x_Q, y_Q, z_Q)$. C, the nucleus centroid, is equal to $(x_C, y_C, z_C)$, and p is the plane parallel to the xy plane passing through Q. Thus, the FLR measure for the point Q is computed using the following formula:

$$FLR(Q) = \sqrt{LR_p^2 - LR_p^2 \times n(p,C)^2 + n(p,C)^2} \times 100\%$$

In this formula, $0 \leq n(p, C) \leq 1$ is the relative distance between the plane p and the centroid C (namely, it is 0 for the plane p passing through the center of the nucleus and is equal to 1 at marginal positions). Moreover, $0 \leq LR_p \leq 1$ is the two-dimensional local radius of the point Q computed at the nucleus cross-section given by p, which is defined as follows:

$$LR_p = \frac{d(C_p, Q)}{d(S, Q) + d(C_p, Q)}$$

$C_p = (x_C, y_C, z_Q)$ is the projection of the point C onto the plane p. S is the closest point to Q at the nucleus surface lying in the plane p, and d(X, Y) denotes the length of the shortest path from point X to Y in the nucleus. Therefore, d(S, Q) is the distance of Q from the nucleus surface in the plane p, and $d(C_p, Q)$ is the length of the shortest path from $C_p$ to Q in the nucleus.

Fluorescence intesity in selected genomic regions was estimated by the use of Andor iQ software (version 1.0.1, ANDOR Technology, South Windsor, CT) and animation was performed by the use of ImageSurfer (http://152.19.37.82/main).

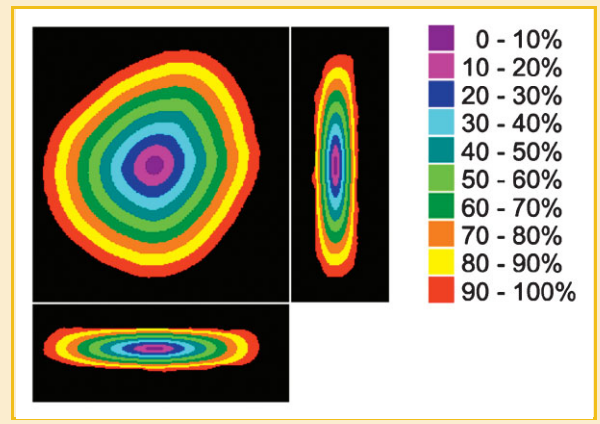


Fig. 2. Example of a local radius map used to determine the nuclear radial distribution of telomeres in flat mouse fibroblasts. Ten layers spanning distances of 10% are visualized in three orthogonal cross-sections of a flat nucleus. The precise position of telomeres in the map (a value in the range of 0–100%) was calculated for each telomere using Acquiarium software.

## STATISTICAL EVALUATION

Data obtained using Acquiarium software [Matula et al., 2009] were statistically evaluated using Statistica 8.0 (StatSoft, Inc.) software. The relative radial distribution of telomeres was evaluated using a non-parametric test, which was necessary due to the data structure (see histogram). The particular test used was the Kruskal–Wallis one-way analysis of variance (ANOVA) by ranks. The null hypothesis was that the median value of the relative radial telomere distribution does not differ among the studied cell lines. The alternative hypothesis was that the median value of the relative radial telomere distribution differs among individual cell lines. The outcomes were determined using an α level of 0.05 (i.e., with maximum 5% chance of making a type I error). Histograms and box plots were created using Statistica 8.0 (StatSoft, Inc.) software and SigmaPlot 8.0 software (Jandel Scientific, CA).

### WESTERN BLOTTING

Cells were washed in PBS and lysed in sodium dodecyl sulphate (SDS) lysis buffer (50 mM Tris–HCl, pH 7.5; 1% SDS; 10% glycerol). All subsequent steps were performed as described previously [Bártová et al., 2005; Harničarová et al., 2006]. Membranes were probed using the following antibodies: rabbit polyclonal antibody to Rap1 (#ab4181, Abcam), anti-Pot1 (H-200) (sc-33789, Santa Cruz Biotechnolgy, Inc.), rabbit polyclonal to TERT (ab23699, Abcam), and mouse monoclonal antibody to PML (#K0196-3, MBL, Medical & Biological Laboratories, Co., LTD). B-type lamins were analyzed using anti-lamin B (sc-6217, Santa Cruz Biotechnology, Santa Cruz, CA). Secondary antibodies included anti-rabbit IgG (A-4914, Sigma, Germany), anti-mouse IgG (A-9044, Sigma), anti-mouse $IgG_1$ (sc-2060, Santa Cruz), and anti-goat IgG (A4174, Sigma). All secondary antibodies were diluted 1:2,000. Detection was performed as already described [Bártová et al., 2005; Galiová et al., 2008].

### ANALYSIS OF TERMINAL RESTRICTION FRAGMENTS—DETECTION OF TELOMERE LENGTH

High molecular weight DNA was isolated from (wt), SUV39h (dn), and LMNA (dn) cells. Approximately $5 \times 10^6$ cells were re-suspended in buffer (1 mM Tris–HCl, pH 6.0; 50 mM EDTA; 0.4 M mannitol), heated to 50°C, supplemented with one volume of 2% (w/v) low melting point agarose (dissolved in 0.4 M mannitol and 0.02 M MES, pH 5.35), and loaded onto the sample mold (Bio-Rad). Plugs were treated with 1 mg/ml proteinase K (dissolved in 0.5 M EDTA and 1% lauroylsarcosine) at 55°C ($2 \times 24$ h incubations) and then sequentially washed in TE buffer (10 ml, $3 \times 20$ min), TE buffer supplemented with 1 mM PMSF (2 ml, $2 \times 1$ h) to inactivate proteinase K, and 0.1× TE buffer at 37°C (10 ml, $5 \times 30$ min). DNA in the plugs was digested with *Hin*fI and *Hae*III (60 U/300 μl) for 16 h. The plugs were then washed for 2 h in TE buffer and for 1 h in 0.5× TBE.

Pulsed field gel electrophoresis was performed using the Gene Navigator System apparatus (GE Healthcare). DNA fragments were separated under the following conditions: 1% agarose in 0.5× TBE; pulses of 2 h/2 s, 17 h/2–20 s, and 1 h/20 s at 180 V; 12°C. The gel was stained with ethidium bromide for 30 min and washed in double distilled water ($2 \times 30$ min washes).

In-gel hybridization was performed with the native gel to visualize telomeric G-strand overhangs. It was then performed on the same gel after denaturation to analyze telomeric repeat length, according to the protocol described by Hemann and Greider [1999]. Briefly, the gel was dried on filter paper at 50°C and pre-hybridized for 1 h at 55°C in hybridization solution (50 mM $NaH_2PO_4$, 5× Denhardt's solution, 5× SSC). Hybridization was performed for 3 h at 55°C in 5 ml of hybridization solution containing $^{32}P$ end-labeled oligonucleotide probe $(CCCTAA)_4$. The gel was washed in 4× SSC at RT ($3 \times 20$ min) and 4× SSC containing 0.1% SDS at 57°C ($3 \times 20$ min). Signals were visualized using FLA 7000 (FUJI FILM). The gel was denatured in 0.6 M NaCl and 0.2 M NaOH for 1 h, and neutralization proceeded for 1 h in 1.5 M NaCl and 0.5 M Tris–HCl, (pH 7.4). Finally, the gel was washed for 30 min in water. Re-hybridization with the same DNA probe was then performed.

### TRANSFECTION OF CELLS WITH AN EXPRESSION VECTOR ENCODING GFP–TRF1

Individual plasmids encoding GFP-hTRF1-pS65T-C1 (generous gift from C.M. Counter, Duke University Medical Center, Durham, NC) were inserted into *E. coli* DH5α for amplification. Plasmid DNA was isolated using the Qiagen Large-Construct kit (#12462, Qiagen, Bio-Consult, Czech Republic). Purified plasmid DNA was then transfected into (wt) and (dn) SUV39h and LMNA MEFs using the METAFECTENE$^{TM}$PRO system (Biontex Laboratories GmbH, Germany). Cells expressing GFP-TRF1 were fixed in 4% paraformaldehyde for 10 min and subjected to standard immunofluorescence staining using mouse monoclonal antibody against to PML (#K0196-3, MBL, Medical & Biological Laboratories, Co., LTD). Cells were counterstained with TO-PRO-3 (0.4 mg/ml).

## RESULTS

### TELOMERES SIGNIFICANTLY ASSOCIATE WITH CHROMOCENTERS IN FIBROBLASTS

In interphase nuclei of mouse cells, pericentromeric regions are arranged into DAPI-positive clusters, called chromocenters [Probst and Almouzni, 2008; see Fig. 1Bb,Bc]. Similarly, we observed clustering of telomeric regions in the mouse genome (Figs. 1Bc and 3A1,A2). Because the mouse karyotype has 20 chromosomes, we expected to observe 80 telomeres. This number was found in only wild type (wt) and (dn) SUV39h interphase cells, however, this count involves telomeric clusters. On metaphase spreads, we have observed approximately 120 individual telomeres in SUV39h (wt) cells and ~170 telomeres in LMNA (wt) fibroblasts. Increased number of telomeres could be caused by cell immortalization that induces aneuploidy. In our experiments, TSA-treated SUV39h (wt) and (dn) cells had levels of telomeric clustering that were significantly different from those of their non-treated counterparts (Fig. 3B, Table I). Specifically, TSA decreased the number of telomeric clusters in SUV39h (wt) cells, while it increased this number in SUV39h (dn) fibroblasts. Both TSA-treated (wt) and (dn) LMNA cells contained a greater number of telomeric clusters than their non-treated counterparts (Fig. 3B, Table I). Number of telomeric clusters could be influenced by cell cycle changes. Cell cycle analysis revealed that only TSA-stimulated SUV39h (wt) cells exhibited a significant increase in cell number at S-G2 phases (compare Figs. 3B and 4), suggesting that genome duplication may have affected the number of telomeric clusters in these cells.

Further analysis of telomeric clusters showed that some clusters were positioned on the periphery of chromocenters (Figs. 1Bc and 3C). The number of telomeric clusters associated with chromocenters was lower in control SUV39h (dn) and LMNA (dn) cells in comparison with their wild type counterparts. TSA-treated LMNA (wt) and LMNA (dn) fibroblasts were also characterized by decreased number of telomeric clusters associated with chromocenters (Fig. 3C). The single exception was TSA-treated SUV39h (dn) fibroblasts, which had a greater number of chromocenter-associated telomeres than control SUV39h (dn) cells (Fig. 3C).

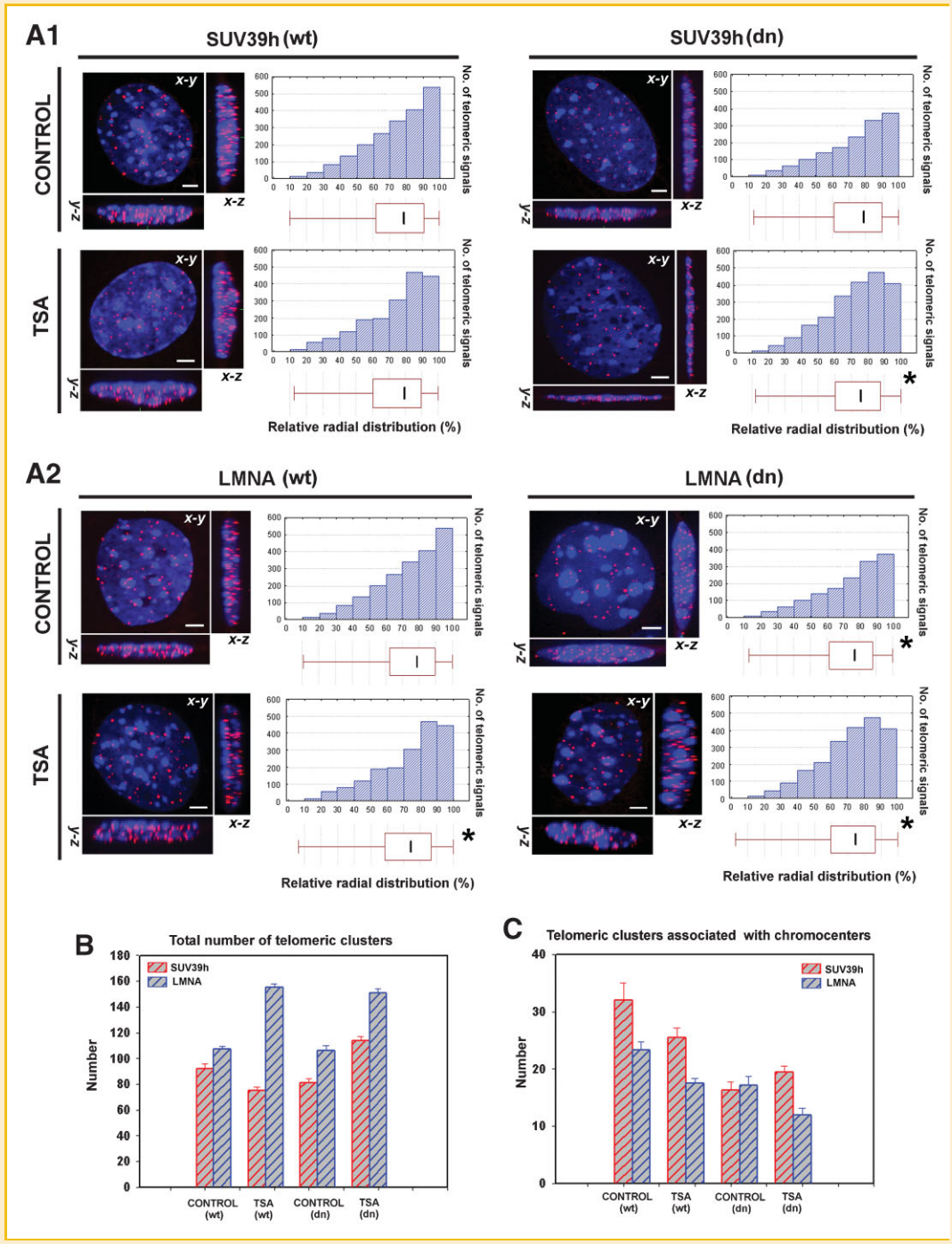


Fig. 3. Telomeric clusters in the SUV39h and LMNA experimental systems. 3D projections of interphase nuclei constructed from 60 optical sections showing telomere distribution in the (A1) SUV39h experimental system and (A2) LMNA experimental system. Bars = 1 μm. Histograms and box plots are shown to the right. In box plots, the line depicts the median, the box the 1st quartile, and the whickers the 3rd quartile. Asterisks indicate significant Kruskal–Wallis *P* values, which are shown in Table III. B: Total number of telomeric clusters (mean ± SEM) in control and TSA-treated SUV39h (wt), SUV39h (dn) fibroblasts as well as in control and TSA-treated LMNA (wt), LMNA (dn) fibroblasts. C: Total number of telomeric clusters associated with chromocenters in the SUV39h and LMNA experimental systems.

## TELOMERE NUCLEAR RADIAL ARRANGEMENT IN SUV39h- AND LMNA-DEFICIENT FIBROBLASTS

The nuclear radial distribution of all telomeres was calculated in SUV39h and LMNA experimental systems (distributions and *P* values provided in Tables II and III, respectively). In (wt) and (dn) SUV39h cells, the median telomere position was ~80% of nuclear the radius, while TSA in SUV39h (dn) cells caused repositioning of telomeres to ~75% of the nuclear radius. The non-parametric Kruskal–Wallis ANOVA test allowed us to reject the null hypothesis that relative radial distributions do not significantly differ in the

TABLE I. Kruskal–Wallis *P* Values for Comparison of Telomere Number in the SUV39h and LMNA Systems

| | SUV39h (wt) | SUV39h (wt) TSA | SUV39h (dn) | SUV39h (dn) TSA |
|---|---|---|---|---|
| SUV39h (wt) | – | 0.021998* | 0.576461* | 0.103879* |
| SUV39h (wt) TSA | 0.021998* | – | 1.00000 | 0.000001 |
| SUV39h (dn) | 0.576461* | 1.000000 | – | 0.000642* |
| SUV39h (dn) TSA | 0.103879* | 0.000001* | 0.000642* | – |
| | **LMNA (wt)** | **LMNA (wt) TSA** | **LMNA (dn)** | **LMNA (dn) TSA** |
| LMNA (wt) | – | 0.000000* | 1.000000 | 0.000022* |
| LMNA (wt) TSA | 0.000000* | – | 0.000006* | 1.000000 |
| LMNA (dn) | 1.000000 | 0.000006* | – | 0.000496* |
| LMNA (dn) TSA | 0.000022* | 1.000000 | 0.000496* | – |

*Statistically significant.

SUV39h experimental system. Multiple comparison testing revealed that the relative radial distributions of telomeres in TSA-treated SUV39h (dn) cells differed significantly from those of the three other SUV39h groups (Table III). Differences in the distribution of telomeres were especially significant between TSA-treated SUV39h (dn) fibroblasts and control SUV39h (wt) fibroblasts ($P = 0.000032$) as well as between TSA-treated and control SUV39h (dn) fibroblasts ($P = 0.001611$, Table III). In the LNMA experimental system, the relative radial telomere distribution differed significantly among experimental groups, with one exception. No differences were noted between TSA-treated LMNA (wt) cells and TSA-treated LMNA (dn) cells (Table III). These SUV39h- and LMNA-related data show that, in majority of cases, TSA caused repositioning of telomeres closer to the nuclear center. This nuclear relocation did not appear to be influenced by changes in the cell cycle profile, as it occurred in both the SUV39h and LMNA experimental system and only TSA-treated SUV39h (wt) cells exhibited a significant increase in the number of S-G2 cells (Fig. 4).

## ASSOCIATION OF TELOMERES WITH PML BODIES IN SUV39h- AND LMNA-DEFICIENT FIBROBLASTS

To investigate the relationship between the telomere-associated protein TRF1 and PML bodies, we performed immunostaining for PML protein variants in cells transiently expressing GFP-TRF1 (Fig. 5A). We observed an association between GFP-TRF1 and PML bodies in ~11 telomeric clusters in SUV39h (wt) cells, ~15 clusters in SUV39h (dn) cells, ~20 clusters in LMNA (wt) cells, and ~12 clusters in LMNA (dn) cells (Fig. 5B). These relative proportions were maintained even when the number of TRF1-positive PML bodies was normalized to the average number of PML bodies in these cells (Fig. 5C). Thus, the percentage of telomeric clusters that associated with PML bodies was ~14% in SUV39h (wt) cells, ~25% in SUV39h

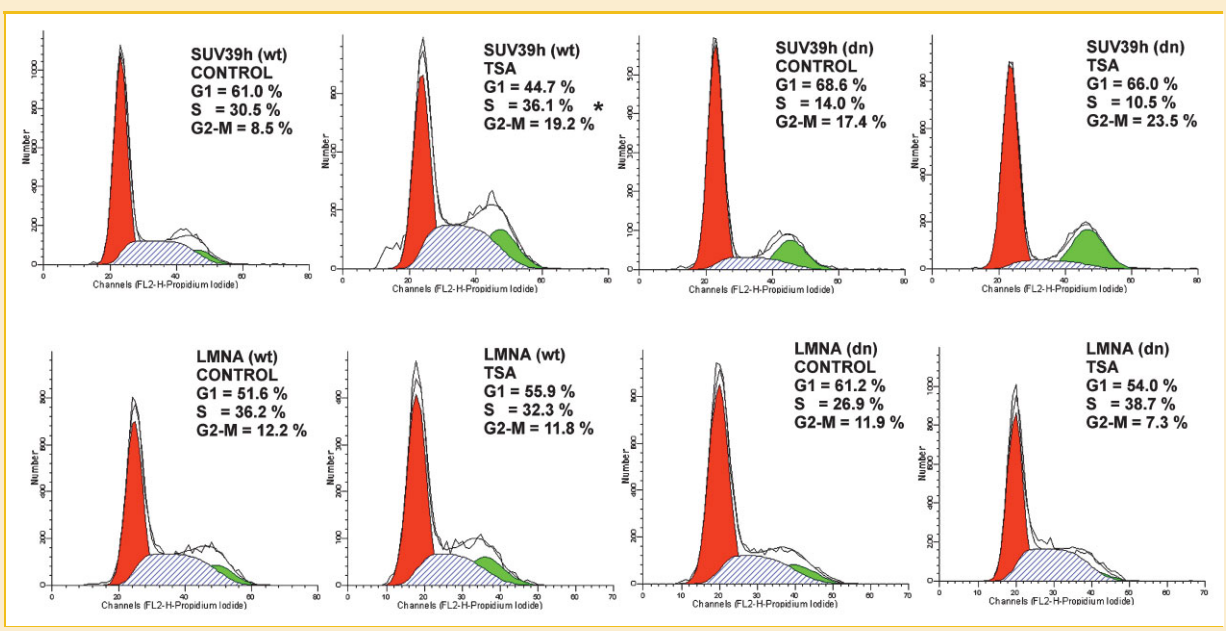


Fig. 4. Flow cytometric analysis of cell cycle profiles in control and TSA-treated SUV39h and LMNA fibroblasts. G1 phase is shown in red, S phase in dashed blue, and G2/M in green. SUV39h (wt) cells and LMNA (wt) cells served as controls for the SUV39h and LMNA-experimental system, respectively. An asterisk indicates that the number of cells in S and G2 phase was higher in TSA-treated cells than the relevant control. Data were analyzed using ModFit software.

TABLE II. Radial Distribution of Telomeres in the SUV39h and LMNA Experimental Systems

| | SUV39h (wt) | SUV39h (wt) TSA | SUV39h (dn) | SUV39h (dn) TSA |
|---|---|---|---|---|
| Median | 78.5% | 79.4% | 79.0% | 75.7% |
| 1 quantile (25th percentile) | 61.2% | 60.5% | 60.1% | 60.5% |
| 2 quantile (75th percentile) | 91.0% | 89.7% | 90.0% | 87.5% |
| Cells (N) | 22 | 22 | 18 | 19 |
| Telomere clusters (N) | 2,015 | z1,624 | 1,461 | 2,160 |
| | LMNA (wt) | LMNA (wt) TSA | LMNA (dn) | LMNA (dn) TSA |
| Median | 78.7% | 74.4% | 76.9% | 74.6% |
| 1 quantile (25th percentile) | 62.4% | 58.6% | 61.6% | 59.6% |
| 2 quantile (75th percentile) | 89.5% | 86.6% | 87.9% | 86.4% |
| Cells (N) | 43 | 40 | 27 | 32 |
| Telomere clusters (N) | 4,610 | 6,208 | 2,862 | 4,837 |

Distances of telomeres from fluorescence gravity center (shown in %) were calculated using Acquiarium software and normalized to the local nuclear radius (see Materials and Methods Section).

(dn) cells, ~44% in LMNA (wt) cells, and ~20% in LMNA (dn) cells. Differences in the percentages in SUV39h (wt) and LMNA (wt) cells may be explained by distinct immortalization conditions. Taken together, our observations imply that SUV39h and LMNA deficiency significantly influence not only clustering of telomeres (Fig. 3B), but also the association of telomere clusters with PML bodies (Fig. 5B,C). Moreover, the number of telomeric clusters was not influenced by cell cycle changes in SUV39h and LMNA experimental systems, owing to the fact that only TSA-treated SUV39h (wt) cells were found to accumulate in S-G2 phases (Fig. 4). For the same reason, changes in co-localization of telomeres and PML bodies were unlikely to be due to the increase in the number of PML bodies that has been shown to occur in S phase [Dellaire et al., 2006; Krejčí et al., 2008]. Generally, telomere co-localization with PML bodies more frequently occurs in telomerase-negative cells, which use an ALT mechanism [Wu et al., 2000]. Conversely, we observed that TRF1-PML association was lower in telomerase-negative SUV39h fibroblasts than in TERT-positive LMNA (wt) fibroblasts (Figs. 5B and 7A). However, TRF1-PML association was increased in SUV39h (dn) fibroblasts, while it was decreased in LMNA (dn) fibroblasts when compared with relevant controls (Fig. 5B,C). These differences in TRF1-PML association are likely related to differing TERT levels in these cells (Fig. 7A).

In addition to investigating the relationship between PML bodies and TRF, we analyzed the interrelationship between PML bodies the other shelterin protein, Rap1. We observed a significant association between Rap1 and PML in SUV39h and LMNA cells (both wt and dn) in the presence and absence of TSA (Fig. 6A). However, Rap1-negative PML bodies were more frequently found after TSA treatment and in SUV39h (dn) cells (see frames in Fig. 6A). Surprisingly, the fluorescence signals for Rap1 (Fig. 6A) were more diffuse than those for GFP-TRF1 (Fig. 5A). This may be due to differences in antibody specificity and/or the presence of Rap1 in non-telomeric TTAGGG repeats, as has been observed for TRF1 in Chinese hamster cells [Krutilina et al., 2003] and for TRF2 associated with the nucleolus [Zhang et al., 2004]. Several antibodies to telomeric proteins other than Rap 1 were also tested in our experiments [TRF1 (sc-1977), Pot1 (sc-33789), and rabbit polyclonal to telomerase (ab23699)]. However, unlike the Rap1 antibody, these antibodies failed to produce an optimal interphase pattern (as seen in Fig. 5A) expected for telomere-associated proteins. In accord with the frequent presence of Rap1-negative PML bodies in SUV39h (dn) cells, Western blot analysis revealed that these cells contained reduced levels of PML protein and Rap1 (Fig. 6B). These data correlated with the frequent absence of Rap1 from PML bodies in SUV39h (dn) cells. Similarly, the level of PML protein was decreased

TABLE III. Kruskal–Wallis *P* Values for Comparison of the Nuclear Radial Distribution of Telomeres in the SUV39h and LMNA Systems

| | SUV39h (wt) | SUV39h (wt) TSA | SUV39h (dn) | SUV39h (dn) TSA |
|---|---|---|---|---|
| SUV39h (wt) | – | 1.000000 | 1.000000 | 0.000032* |
| SUV39h (wt) TSA | 1.000000 | – | 1.000000 | 0.002570* |
| SUV39h (dn) | 1.000000 | 1.000000 | – | 0.001611* |
| SUV39h (dn) TSA | 0.000032* | 0.002570* | 0.001611* | – |
| | LMNA (wt) | LMNA (wt) TSA | LMNA (dn) | LMNA (dn) TSA |
| LMNA (wt) | – | 0.000000* | 0.005653* | 0.000000* |
| LMNA (wt) TSA | 0.000000* | – | 0.000032* | 1.000000 |
| LMNA (dn) | 0.005653* | 0.000032* | – | 0.000471* |
| LMNA (dn) TSA | 0.000000* | 1.000000 | 0.000471* | – |

*Statistically significant.

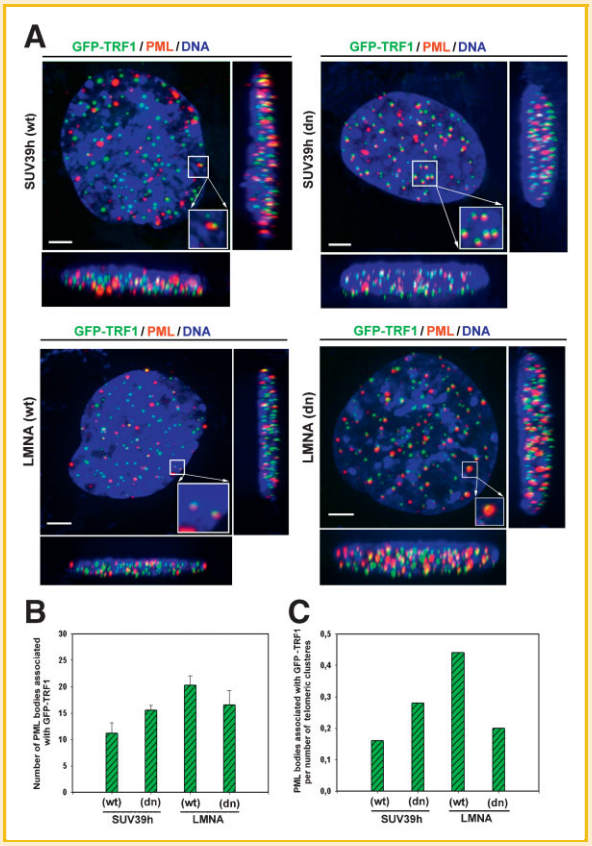


Fig. 5. Co-localization of telomere-associated TRF1 protein with PML bodies. A: Immunofluorescence staining showing an association between GFP-conjugated TRF1 (green) and some PML bodies (red) in SUV39h- and LMNA-deficient cells and their control counterparts. 3D projections were generated using Acquiarium software. Bars = 1 μm. B: Number of PML bodies associated with GFP-TRF1. C: Number of PML bodies associated with GFP-TRF1 normalized to the total number of telomeric clusters.

in TSA-treated LMNA (wt) cells in comparison with relevant control (Fig. 6B).

### GLOBAL CHANGES IN TERT AND POT1 EXPRESSION LEVELS CAUSED BY SUV39h AND LMNA DEFICIENCY

These supplementary experiments showed that Pot1 levels and TERT expression were relatively stable between (wt) and (dn) LMNA cells, even after TSA treatment (Fig. 7A). Interestingly, (wt) and (dn) SUV39h cells contained a much lower level of Pot1 than (wt) and (dn) LMNA counterparts. SUV39h cells also lacked TERT, a finding that may correspond with ALT in this experimental model (Fig. 7A). Surprisingly, analysis of G-strand overhangs by Southern blot did not show changes in the telomere length in either the LMNA or SUV39h experimental system (Fig. 7B). This could be caused by immortalization of the cell lines. This possibility is in agreement with a report by García-Cao et al. [2004] showing that telomere length remains relatively stable in increasing passages of SUV39h (dn) primary MEFs.

## DISCUSSION

Telomeres are the protein-DNA structures that protect ends of eukaryotic chromosomes and are essential for maintaining of chromosome stability. Here, we tested if changes in histone signature and A-type lamin deficiency influence telomere nuclear radial arrangement, including telomere association with PML bodies. We have found that mouse telomeres associate into clusters, especially in SUV39h (dn) and LMNA deficient cells. Thus, this clustering could be dependent on epigenetic processes and lamin A function.

The nuclear arrangement of telomeres has both structural and functional significance, thus we aimed at the study on nuclear radial arrangement of telomeres. Ludérus et al. [1996] reported that telomeres are non-randomly positioned in human cells. Other studies have found that telomeres are present, on average, at 50% of the nuclear radius in T-lymphocytes [Ferguson and Ward, 1992; Vourc'h et al., 1993]. Analysis of p- and q-telomeres of human chromosomes 3, 8, 9, 13, and 19 has revealed that, compared with centromeric sequences, these regions are present on the opposite side of related territories. Moreover, heterologous telomeres have been shown to be tethered [Molenaar et al., 2003; Weierich et al., 2003]. This finding agrees well with our data showing the formation of telomeric clusters (Fig. 3A1,A2,B). However, in the SUV39h and LMNA (wt) cells, the median nuclear positioning of telomeres was ~80% of the nuclear radius, but not 50% as described above (Tables II and III). TSA treatment caused telomeres to become repositioned closer to the nuclear center (median was ~75%, see Table II and histograms in Fig. 3A1,A2). Owing to the fact that telomeres are repositioned closer to the nuclear center after TSA treatment (Fig. 3A1,A2, Tables II and III) and centromeres closer to the nuclear periphery [Taddei et al., 2001; Bártová et al., 2005], our results are in a good agreement with the polar orientation of telomeres and centromeres reported by Amrichová et al. [2003].

A remarkable feature of telomeres is their ability to silence genes [Gottschling et al., 1990; Cryderman et al., 1999]; therefore, nuclear radial positioning of telomeres seems to be highly significant. For example, in yeast, telomeres form clusters that associate with the nuclear periphery [Gotta et al., 1996] and the silencing of genes located in close proximity to telomeric heterochromatin occurs via the telomeric position effect (TPE) [Baur et al., 2001; Koering et al., 2002; Ning et al., 2003]. TPE was described in *Saccharomyces cerevisiae* for telomeres and nearby silent, thus hypoacetylated, HM mating locus [Braunstein et al., 1993]. Not only locus interaction with telomeres, but also several telomere-associated proteins, including Rap1, SIR2, SIR3 and SIR4 and histone acetylation state, mediates silencing of this adjacent gene [Buck and Shore, 1995]. Moreover, similar gene silencing phenomenon was described as position effect variegation (PEV) for centromeric heterochromatin in *Drosophila melanogaster* [Lewis, 1950; Baker, 1968; Henikoff, 1990]. In this context, we observed that some of telomeric clusters were found to associate with centromeric clusters called chromocenters (Figs. 1Bc and 3A1,A2). Thus, this telomere-chromocenter co-localization could be important for gene down-regulation mediated by both telomeric and centromeric silencing mechanisms,

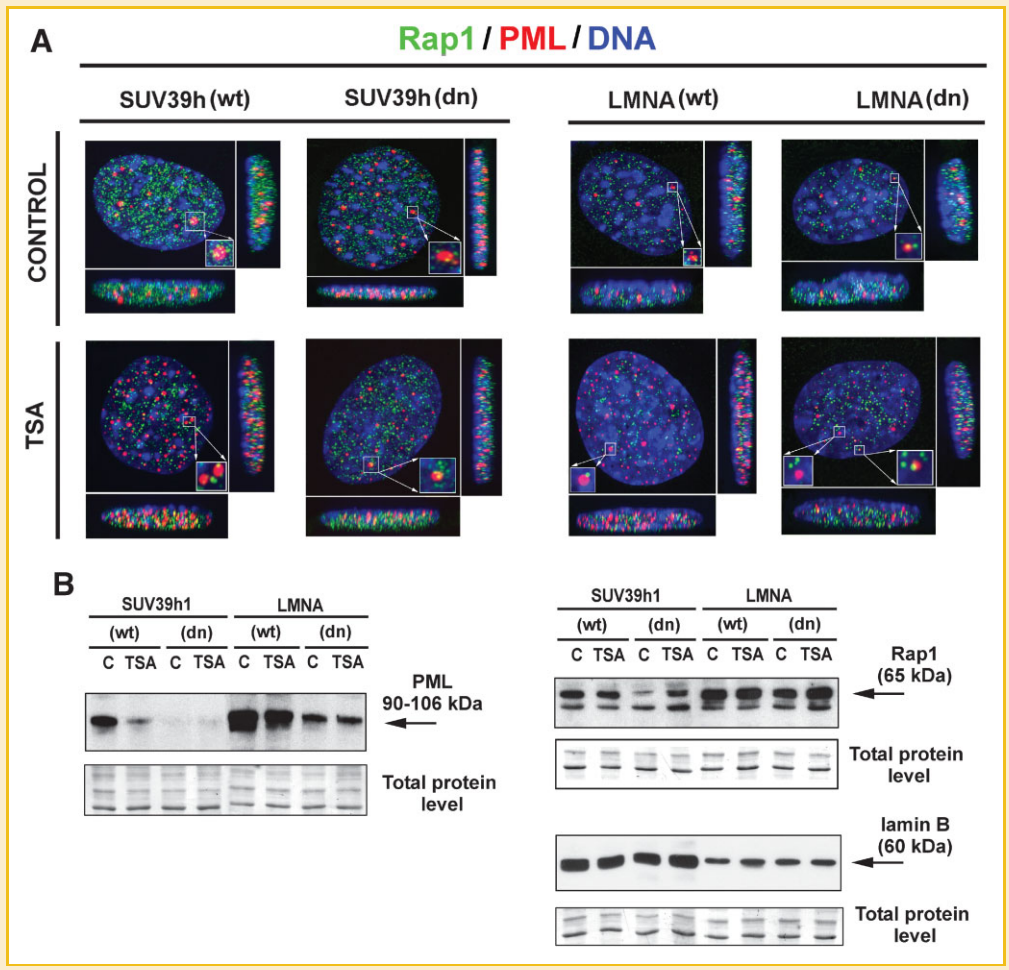


Fig. 6. Association of Rap1 telomeric protein with PML bodies. A: Confocal images of control and TSA-treated (wt) and (dn) SUV39h and LMNA fibroblasts immunostained for Rap1 (green) and PML bodies (red). Note that although Rap1 associated with PML bodies in all groups, this association was less frequently observed after TSA treatment and in SUV39h deficient cells. Bars = 1 μm. B: Western blot analysis of Rap1, PML protein, and lamin B in SUV39h and LMNA experimental systems. Lamin B remained intact in the presence of TSA, showing that it did not undergo apoptotic fragmentation. Individual protein levels were normalized to total protein levels.

as has been described by Baur et al. [2001] and Schübeler et al. [2000].

Telomeres not only play an important role in gene silencing, but also might be attached to the hypothetical nuclear matrix [de Lange, 1992], thus maintain the nuclear architecture. Postberg et al. [2001] clearly described that macromolecular telomeres are associated with the nuclear matrix in vivo and this interaction is mediated by specific telomere-binding proteins, called TEBPs (Shelterin complex), involving TRF1 [Lipps, 1980; Lipps et al., 1982]. The importance of these proteins in telomere-matrix interaction was documented during replication that is characterized by release of telomeres from nuclear matrix owing to interruption of interactions between TEBPs and matrix components. Based on this knowledge, telomeres could be considered as a scaffold for arrangement of chromosome territories within interphase nuclei [Ludérus et al., 1996; Weipoltshammer et al., 1999].

An important aspect of telomeres, influencing their nuclear structure-related properties, is their dynamic positioning in living mammalian cells. As shown by Molenaar et al. [2003], telomeres dynamically associate with relatively immobile PML bodies in human cells. Moreover, both telomeres and centromeres move within the confined nuclear space. Telomere positioning and dynamics has been extensively studied in yeasts that are characterized by telomere movement in restricted volume of nuclei [Hediger et al., 2002]. The velocities of telomeres and centromeres are roughly similar to the velocities of heterochromatin protein 1 (HP1 sub-types which occupy chromocenters), at approximately 0.14 μm/min for HP1 and 0.2 μm/min for telomeres [Molenaar et al., 2003]. This implies that telomere maintenance, optimal shortening, trajectory, and movement are fundamental for the stability of chromosome territories and their domains. These results suggest that telomeres are one of the main chromatin structures that dictate the global architecture of interphase chromatin. Thus, understanding telomere composition, epigenetics, regulation of telomere lengthening, and telomere dynamics will provide clues as to how to protect telomeres against tumor-related end-to-end fusion leading to structural aberrations. Moreover, knowledge of telomere biology may contribute to the design of anti-tumor drugs aimed at

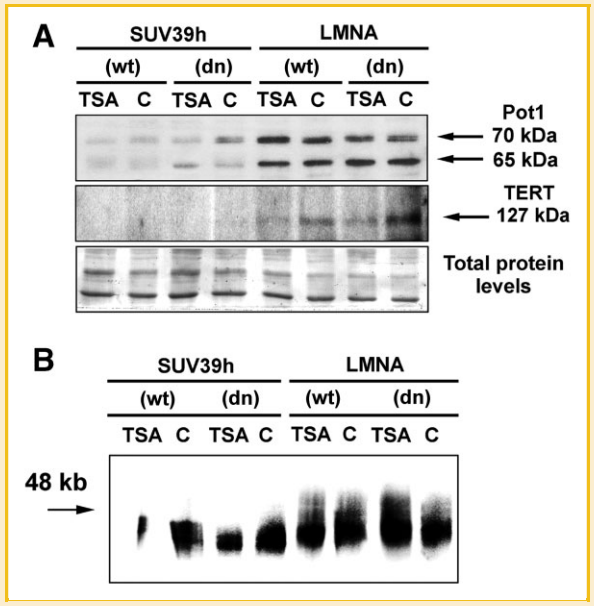


Fig. 7. Telomeric protein levels and telomere length in the SUV39h and LMNA experimental systems. A: Western blot analysis of Pot1 and the telomerase subunit, TERT. B: Southern blot analysis showing that telomere length remains intact in both experimental models.

preventing aberrant telomere function related to the ALT mechanism.

## ACKNOWLEDGMENTS

This work was supported by the research projects LC535, LC06027, 2B06062, ME919, AVOZ50040702, MSM0021622415 and AVOZ50040507. Many thanks to Prof. Thomas Jenuwein (Max-Planck Institute of Immunobiology, Freiburg, Germany) as well as Dr. Teresa Sullivan and Prof. Collin L. Stewart (Institute of Medical Biology in Singapore) for cells. We also thank Dr. C.M. Counter (Duke University Medical Center, Durham, USA) for GFP-TRF1 plasmid. We are also grateful to BioScience Writers Service (Houston, USA) for the critical revision of our manuscript.

## REFERENCES

Amrichová J, Lukášová E, Kozubek S, Kozubek M. 2003. Nuclear and territorial topography of chromosome telomeres in human lymphocytes. Exp Cell Res 289:11–26.

Bailey SM, Cornforth MN, Kurimasa A, Chen DJ, Goodwin EH. 2001. Strand-specific postreplicative processing of mammalian telomeres. Science 293: 2462–2465.

Baker WK. 1968. Position-effect variegation. Adv Genet 14:133–169.

Bártová E, Pacherník J, Harničarová A, Kovařík A, Kovaříková M, Hofmanová J, Skalníková M, Kozubek M, Kozubek S. 2005. Nuclear levels and patterns of histone H3 modification and HP1 proteins after inhibition of histone deacetylases. J Cell Sci 118:5035–5046.

Baur JA, Zou Y, Shay JW, Wright WE. 2001. Telomere position effect in human cells. Science 292:2075–2077.

Blasco MA. 2007a. Telomere length, stem cells and aging. Nat Chem Biol 3:640–649. Review.

Blasco MA. 2007b. The epigenetic regulation of mammalian telomeres. Nat Rev Genet 8:299–309. Review.

Braunstein M, Rose AB, Holmes SG, Allis CD, Broach JR. 1993. Transcriptional silencing in yeast is associated with reduced nucleosome acetylation. Genes Dev 7:592–604.

Buck SW, Shore D. 1995. Action of a RAP1 carboxy-terminal silencing domain reveals an underlying competition between HMR and telomeres in yeast. Genes Dev 9:370–384.

Celli GB, de Lange T. 2005. DNA processing is not required for ATM-mediated telomere damage response after TRF2 deletion. Nat Cell Biol 7:712–718.

Cryderman DE, Morris EJ, Biessmann H, Elgin SC, Wallrath LL. 1999. Silencing at Drosophila telomeres: Nuclear organization and chromatin structure play critical roles. EMBO J 18:3724–3735.

de Lange T. 1992. Human telomeres are attached to the nuclear matrix. EMBO J 11:717–724.

de Lange T. 2004. T-loops and the origin of telomeres. Nat Rev Mol Cell Biol 5:323–329. Review. Erratum in: Nat Rev Mol Cell Biol 2004; 5: 492.

Dellaire G, Ching RW, Dehghani H, Ren Y, Bazett-Jones DP. 2006. The number of PML nuclear bodies increases in early S phase by a fission mechanism. J Cell Sci 119(Pt 6): 1026–1033.

Ferguson M, Ward DC. 1992. Cell cycle dependent chromosomal movement in pre-mitotic human T-lymphocyte nuclei. Chromosoma 101:557–565.

Galiová G, Bártová E, Raška I, Krejčí J, Kozubek S. 2008. Chromatin changes induced by lamin A/C deficiency and the histone deacetylase inhibitor trichostatin A. Eur J Cell Biol 87:291–303.

García-Cao M, O'Sullivan R, Peters AH, Jenuwein T, Blasco MA. 2004. Epigenetic regulation of telomere length in mammalian cells by the SUV39h1 and SUV39h2 histone methyltransferases. Nat Genet 36:94–99.

Gonzalo S, García-Cao M, Fraga MF, Schotta G, Peters AH, Cotter SE, Eguía R, Dean DC, Esteller M, Jenuwein T, Blasco MA. 2005. Role of the RB1 family in stabilizing histone methylation at constitutive heterochromatin. Nat Cell Biol 7:420–428.

Gonzalo S, Jaco I, Fraga MF, Chen T, Li E, Esteller M, Blasco MA. 2006. DNA methyltransferases control telomere length and telomere recombination in mammalian cells. Nat Cell Biol 8:416–424.

Gotta M, Laroche T, Formenton A, Maillet L, Scherthan H, Gasser SM. 1996. The clustering of telomeres and co-localization with Rap1, Sir3, and Sir4 proteins in wild-type Saccharomyces cerevisiae. J Cell Biol 134:1349–1363.

Gottschling DE, Aparicio OM, Billington BL, Zakian VA. 1990. Position effect at S. cerevisiae telomeres: Reversible repression of Pol II transcription. Cell 63:751–762.

Harničarová A, Kozubek S, Pacherník J, Krejčí J, Bártová E. 2006. Distinct nuclear arrangement of active and inactive c-myc genes in control and differentiated colon carcinoma cells. Exp Cell Res 312:4019–4035.

Hediger F, Neumann FR, Van Houwe G, Dubrana K, Gasser SM. 2002. Live imaging of telomeres: yKu and Sir proteins define redundant telomere-anchoring pathways in yeast. Curr Biol 12:2076–2089.

Hemann MT, Greider CW. 1999. G-strand overhangs on telomeres in telomerase-deficient mouse cells. Nucleic Acids Res 27:3964–3969.

Henikoff S. 1990. Position-effect variegation after 60 years. Trends Genet 6:422–426.

Henson JD, Neumann AA, Yeager TR, Reddel RR. 2002. Alternative lengthening of telomeres in mammalian cells. Oncogene 21:598–610.

Ijdo JW, Wells RA, Baldini A, Reeders ST. 1991. Improved telomere detection using a telomere repeat probe (TTAGGG)n generated by PCR. Nucleic Acids Res 19:4780.

Karlseder J, Hoke K, Mirzoeva OK, Bakkenist C, Kastan MB, Petrini JH, de Lange T. 2004. The telomeric protein TRF2 binds the ATM kinase and can inhibit the ATM-dependent DNA damage response. PLoS Biol 2:E240.

Koering CE, Pollice A, Zibella MP, Bauwens S, Puisieux A, Brunori M, Brun C, Martins L, Sabatier L, Pulitzer JF, Gilson E. 2002. Human telomeric position effect is determined by chromosomal context and telomeric chromatin integrity. EMBO Rep 3:1055–1061.

Krejčí J, Harničarová A, Kůrová J, Uhlířová R, Kozubek S, Legartová S, Hájek R, Bártová E. 2008. Nuclear organization of PML bodies in leukaemic and multiple myeloma cells. Leuk Res 32:1866–1877.

Krutilina RI, Smirnova AN, Mudrak OS, Pleskach NM, Svetlova MP, Oei SL, Yau PM, Bradbury EM, Zalensky AO, Tomilin NV. 2003. Protection of internal (TTAGGG)n repeats in Chinese hamster cells by telomeric protein TRF1. Oncogene 22:6690–6698.

Lewis EB. 1950. The phenomenon of position effect. Adv Genet 3:73–115.

Lipps HJ. 1980. In vitro aggregation of the gene-sized DNA molecules of the ciliate Stylonychia mytilus. Proc Natl Acad Sci USA 77:4104–4107.

Lipps HJ, Gruissem W, Prescott DM. 1982. Higher order DNA structure in macronuclear chromatin of the hypotrichous ciliate Oxytricha nova. Proc Natl Acad Sci USA 79:2495–2499.

Ludérus ME, van Steensel B, Chong L, Sibon OC, Cremers FF, de Lange T. 1996. Structure, subnuclear distribution, and nuclear matrix association of the mammalian telomeric complex. J Cell Biol 135:867–881.

Lundblad V. 2002. Telomere maintenance without telomerase. Oncogene 21:522–531. Review.

Matula Pa, Maška M, Daněk O, Matula Pe, Kozubek M. 2009. Acquiarium: Free software for the acquisition and analysis of 3d images of cells in fluorescence microscopy. IEEE Int Symp Biomed Imaging 6:1138–1141.

Molenaar C, Wiesmeijer K, Verwoerd NP, Khazen S, Eils R, Tanke HJ, Dirks RW. 2003. Visualizing telomere dynamics in living mammalian cells using PNA probes. EMBO J 22:6631–6641.

Muntoni A, Reddel RR. 2005. The first molecular details of ALT in human tumor cells. Hum Mol Genet 2:R191–R196. Review.

Nagele RG, Velasco AQ, Anderson WJ, McMahon DJ, Thomson Z, Fazekas J, Wind K, Lee H. 2001. Telomere associations in interphase nuclei: Possible role in maintenance of interphase chromosome topology. J Cell Sci 114(Pt 2): 377–388.

Ning Y, Xu JF, Li Y, Chavez L, Riethman HC, Lansdorp PM, Weng NP. 2003. Telomere length and the expression of natural telomeric genes in human fibroblasts. Hum Mol Genet 12:1329–1336.

Otsu N. 1979. A threshold selection method from gray-level histograms. IEEE Trans Syst Man Cybern 9:62–66.

Postberg J, Juranek SA, Feiler S, Kortwig H, Jönsson F, Lipps HJ. 2001. Association of the telomere-telomere-binding protein complex of hypotrichous ciliates with the nuclear matrix and dissociation during replication. J Cell Sci 114(Pt 10):1861–1966.

Probst AV, Almouzni G. 2008. Pericentric heterochromatin: Dynamic organization during early development in mammals. Differentiation 76:15–23.

Scaffidi P, Misteli T. 2006. Lamin A-dependent nuclear defects in human aging. Science 312:1059–1063.

Schotta G, Lachner M, Sarma K, Bert A, Sengupta R, Reuter G, Reinberg D, Jenuwein T. 2004. A silencing pathway to induce H3-K9 and H4-K20 trimethylation at constitutive heterochromatin. Genes Dev 18:1251–1262.

Schübeler D, Francastel C, Cimbora DM, Reik A, Martin DI, Groudine M. 2000. Nuclear localization and histone acetylation: A pathway for chromatin opening and transcriptional activation of the human beta-globin locus. Genes Dev 14:940–950.

Shumaker DK, Dechat T, Kohlmaier A, Adam SA, Bozovsky MR, Erdos MR, Eriksson M, Goldman AE, Khuon S, Collins FS, Jenuwein T, Goldman RD. 2006. Mutant nuclear lamin A leads to progressive alterations of epigenetic control in premature aging. Proc Natl Acad Sci USA 103:8703–8708.

Soille P. 2004. Morphological image analysis, principles and applications. 2nd edition. Heidelberg: Springer.

Taddei A, Maison C, Roche D, Almouzni G. 2001. Reversible disruption of pericentric heterochromatin and centromere function by inhibiting deacetylases. Nat Cell Biol 3:114–120.

van Steensel B, Smogorzewska A, de Lange T. 1998. TRF2 protects human telomeres from end-to-end fusions. Cell 92:401–413.

Vourc'h C, Taruscio D, Boyle AL, Ward DC. 1993. Cell cycle-dependent distribution of telomeres, centromeres, and chromosome-specific subsatellite domains in the interphase nucleus of mouse lymphocytes. Exp Cell Res 205(1):142–151.

Weierich C, Brero A, Stein S, von Hase J, Cremer C, Cremer T, Solovei I. 2003. Three-dimensional arrangements of centromeres and telomeres in nuclei of human and murine lymphocytes. Chromosome Res 11:485–502.

Weipoltshammer K, Schöfer C, Almeder M, Philimonenko VV, Frei K, Wachtler F, Hozák P. 1999. Intranuclear anchoring of repetitive DNA sequences: Centromeres, telomeres, and ribosomal DNA. J Cell Biol 147: 1409–1418.

Wu G, Lee WH, Chen PL. 2000. NBS1 and TRF1 colocalize at promyelocytic leukemia bodies during late S/G2 phases in immortalized telomerase-negative cells. Implication of NBS1 in alternative lengthening of telomeres. J Biol Chem 275:30618–30622.

Yeager TR, Neumann AA, Englezou A, Huschtscha LI, Noble JR, Reddel RR. 1999. Telomerase-negative immortalized human cells contain a novel type of promyelocytic leukemia (PML) body. Cancer Res 59:4175–4179.

Zhang S, Hemmerich P, Grosse F. 2004. Nucleolar localization of the human telomeric repeat binding factor 2 (TRF2). J Cell Sci 117(Pt 17):3935–3945.